Study on the Bending Behavior of Sandwich Composite Beams

Pedro Miguel Grifo Belbute

Advisor: Professor Manuel José Moreira de Freitas

Co-advisor: Professor Aurélio Lima Araújo

Instituto Superior Técnico

Abstract

Nowadays, the use of composite laminates structures in the automobile, railroad, civil, aeronautical, space and naval industries is growing at a huge rate. Recently, there's been a renewed interest in sandwich laminate structures, whose bending capability and performance is much better when compared to classical laminates. Sandwich structures, which are mainly used as bending components, are formed by materials with very different resistance in the faces and in the core. Therefore the behavior of such structures under bending conditions does not fit the classical laminate theories. Despite this, sandwich structures are simple enough to allow simplified analysis, whose mathematical accuracy depends greatly on the structure itself. In this master's thesis the goal is to study the application of different analysis techniques on sandwich beams under bending conditions using a mixed layerwise approach, by considering a Higher-Order Shear Deformation Theory (HSDT) to represent the displacement field of the viscoelastic core and a First-Order Shear Deformation Theory (FSDT) for the face layers and compare it with simplified theories of Equivalent Single Layers (ESL), such as the Classical Theory (CLPT) and First-Order theories (FSDT). The results obtained through this theory are compared and validated with values retrieved experimentally and numerically by a 3-D finite element and by a higher-order plate element. The advantages relative to the Classical Plate Theory and First-Order Shear Deformation Theory are also analyzed.

Keywords: Sandwich Structure, High Shear Deformation Theory, Finite Elements, 3 point bending, 4 point bending.

1. Introduction

Sandwich structures are formed by two exterior faces which are relatively thin but of high structural stiffness and a much thicker core, which is lighter but less stiff than the faces. The faces and core are bonded using adhesives.

There are many ways to combine materials for the construction of sandwich structures. This allows optimization in accordance with the needs in engineering projects. In the faces the most used materials are steel, aluminum, wood, and laminated composites of carbon fibers, fiberglass, etc. In the core, cork, balsa wood, polymeric foams such as polyurethane, polystyrene, phenolic resin, metallic or carbon honeycombs, amongst others, are the most used materials **[1, 2]**.

The World War II Mosquito aircraft was the first major application of sandwich panels but there were a few earlier, uses of the sandwich principle. By about 1960, especially with the landing of the Apollo capsule on the Moon in 1969 (which used sandwich shells with honeycomb cores), increasing numbers of alternative uses were being discovered, such as in the building, refrigerated storage, automobile and shipbuilding industries **[2]**.

Nowadays sandwich structures can be found in many different industries. One example is the the Swedish company Stena Line which is considering the possibility of modifying their HSS-900 catamaran made of aluminum by a sandwich superstructure that would result in a loss of weight of $2.9\ kg/m^2$ **[3]**. Other examples are the Boeing 787 and the Airbus A350 XWB, built with 50% and 53% of composite materials (including sandwich structures) respectively, which would result, amongst other factors, in a decrease in fuel consumption of 20% and 30%, respectively **[3, 5]**. Also in the civil industries the interest with these structures has been increasing, namely in the renovation of steel bridge decks. Due to fatigue problems these bridges need to replace their decks with a new Sandwich Plate System (SPS) **[6, 7, 8]**.

The usage of sandwich arose from the need to combine a high mechanical stiffness with a lightweight structure. This is achieved by increasing the distance between the faces which leads to an increase in the inertial moment and therefore augmenting the bending stiffness of the structure. With this in mind a sandwich construction can be compared with an I beam, where the faces correspond to the flanges supporting the axial stresses caused by bending moments, and the core works as the web carrying the shear stresses caused by transverse forces and torsion. Despite this, the cores aren't usually stiff enough, resulting in the appearance of shear effects that can't be neglected.

Sandwich panels and beams are therefore simple structures with much better performance than classical laminates under bending conditions. They can be analyzed using simple structural mechanics kinematics, although they are formed by a flexible and viscoelastic core which does not allow the utilization of conventional beam and plate theories. Because of this, arises the need to use models of High-Order Shear Deformation Theory.

This is the main goal of this master's thesis which will be centered in the validation of a new beam finite element model, formulated using a mixed layerwise approach, by considering a Higher-Order Shear Deformation Theory (HSDT) to represent the displacement field of the viscoelastic core and a First-Order Shear Deformation Theory (FSDT) for the displacement field of the face layers. It will then be compared with simplified theories of Equivalent Single Layers (ESL), 3-D finite elements, a higher-order layerwise plate model, and experimental results of 3 and 4 point bending tests in accordance with ASTM regulations. Because of their importance in sandwich structures, longitudinal and shear strains distributions will be presented, especially in the core, since its behavior is mostly viscoelastic. This viscolelastic behavior is very critical and greatly affected by temperature and time variations. Although this is not the main subject, such phenomena will be presented and briefly discussed. The zig-zag effects as a consequence to material discontinuities between faces and core will also be quantified.

2. Hybrid Sandwich Beam Model

The development of a layerwise finite element model is presented here. The basic assumptions in the development of the sandwich beam model are the same as the ones used by Araújo *et al.* **[9]**:

1) All points on a normal to the plate have the same transverse displacement $w(x, y, t)$, where t denotes time, and the origin of the *z* axis is the mid-plane of the core layer;
2) No slip occurs at the interfaces between layers;
3) The displacement is C^0 along the interfaces;
4) Elastic layers are modeled with first order shear deformation theory (FSDT) and viscoelastic core with a higher order shear deformation theory (HSDT);
5) All materials in the core are linear, homogeneous and orthotropic and the elastic layers (faces) are made of laminated composite materials;

Contrary to the model used by *Araújo et al.* **[9]**, which developed this model for a plate element, in the present work the goal is to study the behavior of sandwich beams, therefore it will only be considered the axial, x, and transverse, z, directions in the development of this model.

The FSDT displacement field of the face layers may be written in the general form:

$$\begin{aligned} u^k(x, y, z, t) &= u_0^k(x, y, t) + (z - \bar{z}_k)\theta_x^k(x, y, t) \\ w^k(x, y, z, t) &= w_0(x, y, t) \end{aligned} \tag{1}$$

Where u_0^k is the in-plane displacement of the mid-plane of the layer, θ_x^k are rotations of normals to the mid-plane about the *y* axis (anticlockwise) w_0 is the transverse displacement of the layer (same for all layers in the sandwich), $\bar{z}_k$ is the *z* coordinate of the mid-plane of each layer, with reference to the core layer mid-plane ($\bar{z}_c = 0$) and $k = t, b$ is the layer index **[9]**.

For the viscoelastic core layer, the HSDT displacement field is written as a second order Taylor series expansion of the in-plane displacements in the thickness coordinate, with constant transverse displacement:

$$\begin{aligned} u^c(x, y, z, t) &= u_0^c(x, y, t) + z\theta_x^c(x, y, t) + z^2 u_0^{*c}(x, y, t) + z^3\theta_x^{*c}(x, y, t) \\ w^c(x, y, z, t) &= w_0(x, y, t) \end{aligned} \tag{2}$$

Where u_0^c is the in-plane displacement of the mid-plane of the layer, θ_x^c are rotations of normals to the mid-plane about the *y* axis (anticlockwise) w_0 is the transverse displacement of the layer (same for all layers in the sandwich), c is the layer index. The functions u_0^{*c} and θ_x^{*c} are higher-order terms in the series expansion, defined also in the mid-plane of the core layer **[9]**.

2.1. Formulation

As shown in figure 4 the displacement continuity at the layer interfaces can be written as:

$$u^c\left(x, y, \frac{h_c}{2}, t\right) = u^t\left(x, y, \bar{z}_t - \frac{h_t}{2}, t\right) \tag{3.a}$$

$$u^c\left(x, y, -\frac{h_c}{2}, t\right) = u^b\left(x, y, \bar{z}_b + \frac{h_b}{2}, t\right) \tag{3.b}$$

Where the coordinates of layer mid-planes are:

$$\bar{z}_t = \frac{h_c}{2} + \frac{h_t}{2} \tag{4.a}$$

$$\bar{z}_c = 0 \tag{4.b}$$

$$\bar{z}_b = -\frac{h_c}{2} - \frac{h_b}{2} \tag{4.c}$$

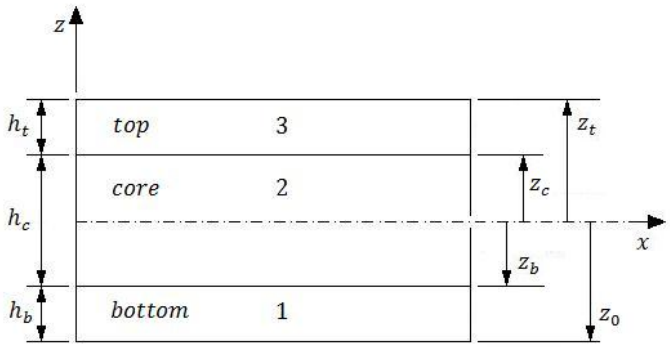

Figure 1: *Sandwich beam model*.

The constitutive relations of the beam model are given as:

$$\begin{Bmatrix}\sigma_{11}\\ \sigma_{13}\end{Bmatrix}^k = \begin{bmatrix}C_{11} & 0\\ 0 & C_{55}\end{bmatrix}^k \begin{Bmatrix}\varepsilon_{11}\\ \gamma_{13}\end{Bmatrix}^k \tag{5}$$

With:

$$C_{11} = \frac{E_1}{1-\upsilon_{12}\upsilon_{21}}, \quad C_{55} = G_{13} \tag{6.a}$$

for orthotropic materials. Where $E_1$is elasticity modulus in the principal direction (1) of the laminate, and E_2 is elasticity modulus in the secondary direction (2). υ_{12} is the Poisson coefficient and $\upsilon_{21} = \upsilon_{12}\frac{E_2}{E_1}$. Finally G_{23}, G_{13} e G_{12} are the shear modulus.

And for isotropic materials:

$$C_{11} = C_{22} = \frac{E}{1-\upsilon^2}, \quad C_{44} = C_{55} = C_{66} = G = \frac{E}{2(1+\upsilon)} \tag{6.b}$$

Where E is the elasticity modulus and υ the Poisson coefficient.

The strain field is given by the displacement field as:

$$\begin{Bmatrix}\varepsilon_{xx}\\ \gamma_{xz}\end{Bmatrix}^k = \begin{bmatrix}\frac{\partial}{\partial x} & 0\\ \frac{\partial}{\partial z} & \frac{\partial}{\partial x}\end{bmatrix} \begin{Bmatrix}u\\ w\end{Bmatrix}^k \tag{7}$$

2.2. Core

The linear strains associated with the assumed displacement field for the viscoelastic core layer are:

$$\begin{cases}\varepsilon_{xx} = \dfrac{\partial u_0^c}{\partial x} + z\dfrac{\partial \theta_x^c}{\partial x} + z^2\dfrac{\partial u_0^{*c}}{\partial x} + z^3\dfrac{\partial \theta_x^{*c}}{\partial x}\\ \gamma_{xz} = \theta_x^c + 2zu_0^{*c} + 3z^2\theta_x^{*c} + \dfrac{\partial w_0}{\partial x}\end{cases} \tag{8}$$

2.3. Faces

Applying the continuity conditions given by (3.a) and (3.b), one obtains for the top face:

$$u_0^c + \frac{h_c}{2}\theta_x^c + \frac{{h_c}^2}{4}u_0^{*c} + \frac{{h_c}^3}{8}\theta_x^{*c} = u_0^t + \left(\bar{z}_t - \frac{h_t}{2} - \bar{z}_t\right)\theta_x^t \tag{9.a}$$

$$\Rightarrow \theta_x^t = -\frac{2}{h_t}u_0^c + \frac{2}{h_t}u_0^t - \frac{h_c}{h_t}\theta_x^c - \frac{{h_c}^2}{2h_t}u_0^{*c} - \frac{{h_c}^3}{4h_t}\theta_x^{*c} \tag{9.b}$$

And for the bottom face:

$$u_0^c - \frac{h_c}{2}\theta_x^c + \frac{{h_c}^2}{4}u_0^{*c} - \frac{{h_c}^3}{8}\theta_x^{*c} = u_0^b + \left(\bar{z}_b + \frac{h_b}{2} - \bar{z}_b\right)\theta_x^b \tag{10.a}$$

$$\Rightarrow \theta_x^b = \frac{2}{h_b}u_0^c - \frac{2}{h_b}u_0^b - \frac{h_c}{h_b}\theta_x^c + \frac{{h_c}^2}{2h_b}u_0^{*c} - \frac{{h_c}^3}{4h_b}\theta_x^{*c} \tag{10.b}$$

The linear strains associated with the assumed displacement field for the face layers are:

$$\begin{cases} \varepsilon_{xx}^k = \dfrac{\partial u_0^k}{\partial x} + z\dfrac{\partial \theta_x^k}{\partial x} - \bar{z}_k\dfrac{\partial \theta_x^k}{\partial x} \\ \gamma_{xz}^k = \theta_x^k + \dfrac{\partial w_0}{\partial x} \end{cases} \tag{11}$$

2.4. Finite element formulation

Using the principle of minimum potential energy:

$$\Pi_k = U_k + W \tag{12}$$

Where Π_k is the potential energy of each layer and $U_k$and W are, respectively, the energy associated with strains in each layer and the work done by externally applied loads:

$$U_k = \frac{1}{2}\int_\Omega \{\varepsilon^k\}^T\{\sigma^k\}d\Omega \tag{13.a}$$

$$W = -\left(\int_\Omega \{d\}^T\{f_b\}d\Omega + \int_S \{d\}^T\{f_s\}dS + \{d\}^T\{f_c\}\right) \tag{13.b}$$

Where ε^k e σ^k are the components of the displacement and tension fields in (7), $\{d\}$, $\{f_b\}$, $\{f_s\}$ and $\{f_c\}$ are the vector of mechanical DOF, the vector of applied loads in the body, the vector of surface tractions and the vector of concentrated forces, respectively. Finally, Ω and S represent, respectively, the volume and surface domains of the beam **[9]**.

The displacement field can be given as

$$\{\boldsymbol{u^k}\} = [Z]^k\{d\} \tag{14}$$

Where the vector of mechanical DOF, after reducing the unknowns through continuity conditions given by (9.b) and (10.b), is:

$$\{d\} = \{u_0^c \quad u_0^t \quad u_0^b \quad w_0 \quad \theta_x^c \quad u_0^{*c} \quad \theta_x^{*c}\}^T \tag{15}$$

And $[Z]^k$ are the matrices obtained using equations (1) and (2), along with equations (9.b) and (10.b).

Carrying on the integration in the thickness direction in equations (13.a) and (13.b) and substituting the results in equation (12), one obtains the variational equation of motion for the sandwich beam, whose solution was obtained through the finite element model using a two-node element with 7 mechanical DOF per node with:

$$\{d^e\} = \sum_{i=1}^{NN}[N_i]\{d_i^e\} = [N]\{a^e\} \tag{16}$$

Where NN is the number of nodes in the element and $[N]$ contains the C^0 shape functions **[12]**:

$$N_1 = 1 - \frac{x}{h_e}$$
$$N_2 = \frac{x}{h_e} \tag{17}$$

Where h_e is the element length.

The strains are related to the element DOF through:

$$\{\varepsilon_m^e\}^k = \sum_{i=1}^{NN} [B_{mi}]^k \{d_i^e\} = [B_m]^k \{a^e\}$$
$$\{\varepsilon_b^e\}^k = \sum_{i=1}^{NN} [B_{bi}]^k \{d_i^e\} = [B_b]^k \{a^e\} \tag{18}$$
$$\{\varepsilon_s^e\}^k = \sum_{i=1}^{NN} [B_{si}]^k \{d_i^e\} = [B_s]^k \{a^e\}$$

Where B_m, B_b and B_s are strain matrices that can be obtained from the shape functions and their derivatives, and are calculated on a layer-by-layer basis.

It is now possible to build the equilibrium equation in matrix form:

$$[K_{uu}^e]\{a^e\} = \{F_u^e\} \tag{19}$$

Where K is the stiffness matrix of the element given by **[9, 10]**:

$$[K_{uu}^e] = \sum_{k=c,t,b} \int_{-1}^{1} \big([B_m^e]^{k^T} [D_m]^k [B_m^e]^k + [B_b^e]^{k^T} [D_c]^k [B_m^e]^k + [B_m^e]^{k^T} [D_c]^k [B_b^e]^k + [B_b^e]^{k^T} [D_b]^k [B_b^e]^k + [B_s^e]^{k^T} [D_s]^k [B_s^e]^k \big) det[J]\, d\xi \tag{20}$$

Where ξ is the natural coordinate of the element and J is the Jacobian of the transformation. $[D_m]$, $[D_c]$, $[D_b]$ and $[D_s]$ are the constitutive matrices with the membrane, coupled, bending and shear contributions, respectively.

Shear locking was avoided using reduced integration in the construction of the stiffness matrices **[11, 12]**.

3. Validation of the model

After implementation of the model using Matlab® for manipulation, construction of matrices and various other operations, such as resolution of the equations system and post process of the results, the objective was to compare the results with other existing models and experimental results. The beams were discretized in 40 elements, since the solution had already converged for 20 elements.

3.1.3 Point bending tests

In this case the goal was to make a comparative analysis from the developed beam model with other models and theories, calculating the mid-span displacement of a beam under three point bending loads in accordance with ASTM-C393 **[13].**

The other two models for comparison were the Classical Laminate Plate Theory (CLPT) and a Simplified Sandwich Beam Theory (SSBT) **[14]**, implemented in finite elements by *Sainsbury* et al. **[15]**. All the results are adimensionalized relative to the CLPT values.

Several elasticity modulus in the core were tested, as well as different $\frac{L}{h_T}$ ratios, where L is the beam length and h_T is the total thickness of the beam. The most relevant properties for these tests are given in table 1.

$\boldsymbol{P}$	$10\ N$
$\boldsymbol{E_t = E_b}$	$69\ GPa$
$\boldsymbol{v}$	0.3

Table 1: Data for the beam analysis.

3.1.1. Results and discussion

The results for obtained for these tests are given in figure 2:

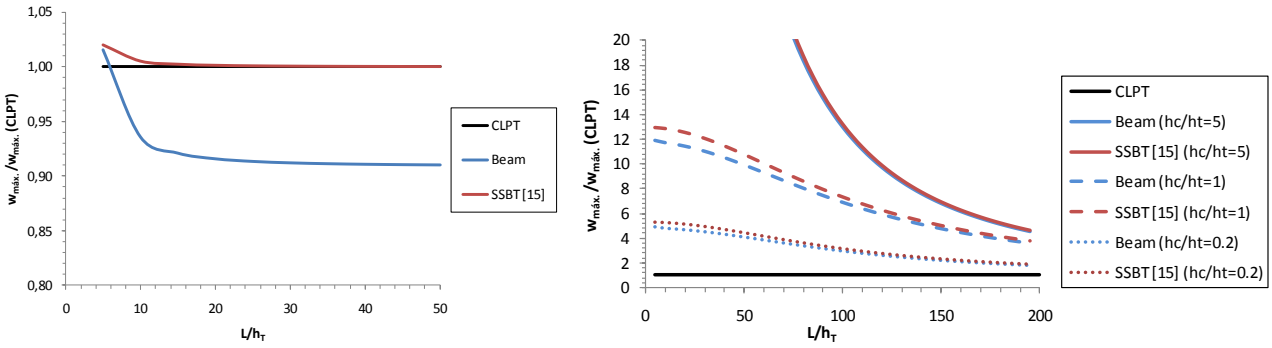

$a)\ E_c = 69\ GPa$ $b)\ E_c = 0.069 \times 10^{-3}\ GPa$

Figure 2: Mid-span displacement relative to the classical theory for different $\frac{\mathbf{h_c}}{\mathbf{h_t}}$ ratios.

As it can be seen from figure 2.a) the beam and SSBT models are very close to the classical results when the core as the same rigidity as the faces. The maximum error of the beam model is 9%. When the elastic modulus of the core decreases the convergence to the classical values takes place at bigger $\frac{L}{h_T}$ ratios (Figure 2.b)). This is justified by the shear effects, namely the transverse distortion, that is more severe in the configuration of short beams and also tends to increase when the elastic modulus of the core decreases. Another aspect is that the classical theory does not predict the shear effects, thus contributing for a bigger discrepancy between models. The relative thickness is also important since for bigger $\frac{h_c}{h_t}$ ratios the shear effects will be more significant as a consequence of the increase in thickness of the core.

3.2.4 Point Bending tests with application in bridge decks

The goal was to compare experimental and 3-D FEM results obtained by Teixeira de Freitas et al. **[6],** for the application of a SPS system in Dutch bridge decks, with the presented beam model as well as the SSBT and a higher-order layerwise plate element by Araújo *et al.* **[9]**.

The beam specimens characteristics used in these tests are presented in table 2:

Specimen	$h_b\ (mm)$	$h_c\ (mm)$	$h_t\ (mm)$	$\frac{h_c}{h_f}$
S12305	12	30	5	3.5
S12155	12	15	5	1.8
S12206	12	20	6	2.2
S12306	12	30	6	3.3
S10306	10	30	6	3.8

Tabela 2: Specimens characteristics.

Steel Grade S355 was selected for both steel faces. The sandwich core is polyurethane (solid polymer) with a density of 1150 kg/m^3 and a Poisson coefficient of 0.36, manufactured by Elastogran GmbH. The core material was first tested by Teixeira de Freitas et al. **[6]** for the three temperatures and the mean values obtained are shown in table 4. The steel faces properties are given in table 3.

	S355
σ_{ced}	355 MPa
σ_R	510 MPa
E	210 GPa
υ	0.3

Tabela 3: S355 steel properties.

Temperature	$E\ (MPa)$	$\sigma_{ced}\ (MPa)$
-10ºC	1049	22
RT	721	25
50ºC	471	17.7

Tabela 4: Core properties.

3.2.1. Experimental Procedure

The tests were conducted under three different temperatures (-10ºC, Room Temperature (RT) and +50ºC), in accordance with ISO-527 (1996) **[16],** in order to test the core behavior when subject to real conditions.

For these 4 point bending tests *Teixeira de Freitas et al.* **[6]**, two types of load configuration were used: short and long beams. The short beam's load configuration was quarter point loading with 400 mm support span and 200 mm load span. The long beam's load configuration was third point loading with 750 mm support span and 250 mm load span. Figure 3 shows both load configurations.

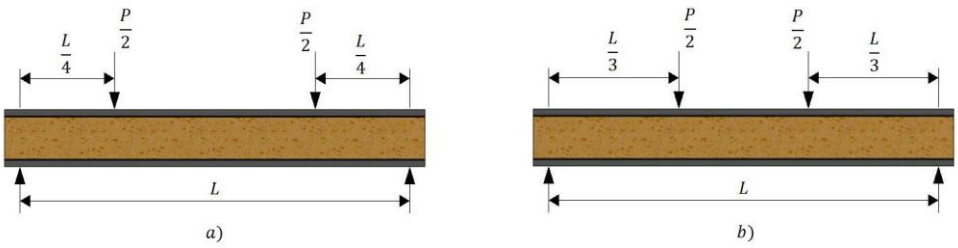

Figure 3: Four point bending tests configuration in accordance with ASTM-C393: a) Short beams loading; b) Long beams loading.

3.2.2. Results and discussion

The rigidity values K, ($K = \frac{load}{displacement}$), obtained for the long beam configuration at -10ºC and 50ºC are presented in Figure 4.

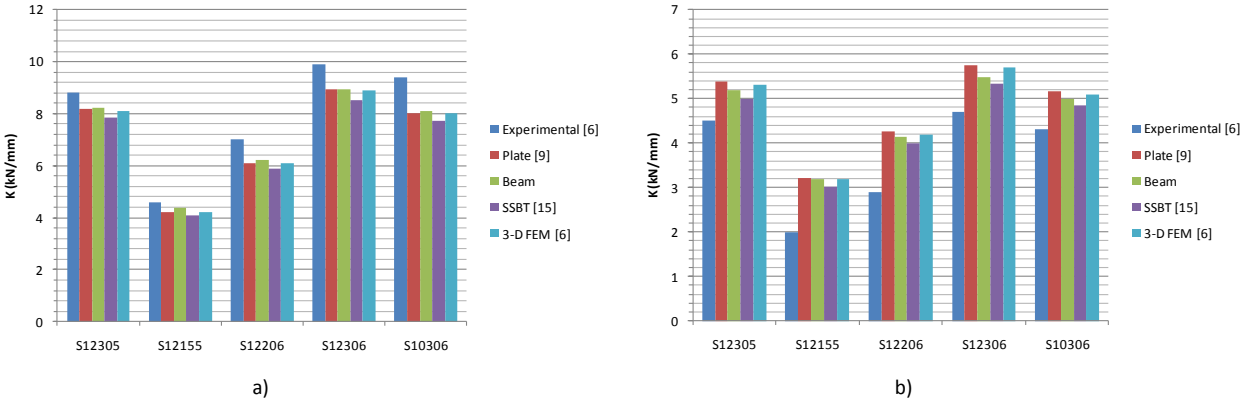

Figure 4: Comparison of rigidity values obtained at long beam configuration for experimental tests and for beam, plate, SSBT and 3-D elements at a) -10ºC; b) 50ºC.

Figure 5 shows the rigidity values obtained for the short beam configuration at -10ºC and 50ºC.

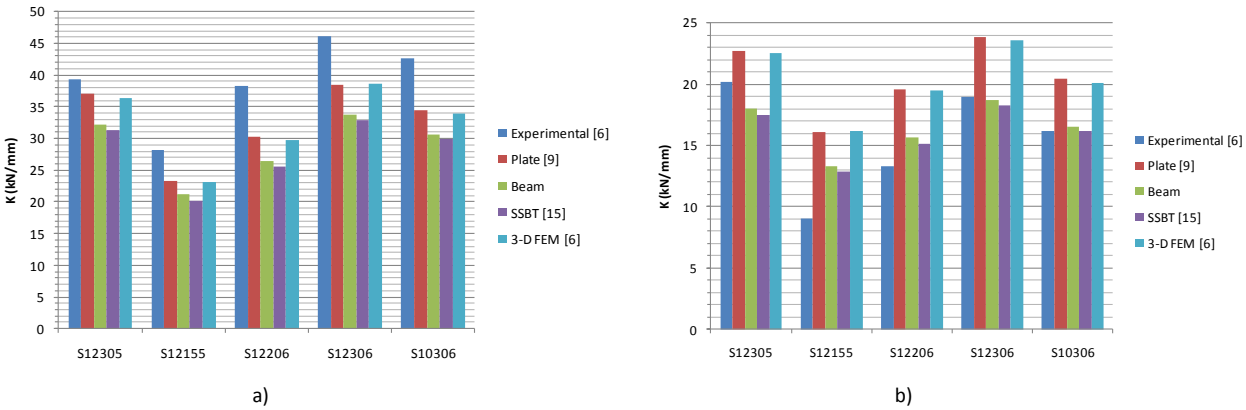

Figure 5: Comparison of rigidity values obtained at short beam configuration for experimental tests and for beam, plate, SSBT and 3-D elements at a) -10ºC; b) 50ºC.

It can be concluded that for long beam configuration at -10ºC, i.e., for bigger core rigidity, the beam element results are much closer to the experimental values as well as the plate and 3-D elements. Comparatively to the SSBT element the beam element guarantees an improvement in the error of about 5%. For 50ºC the same behavior remains between elements but the experimental results decrease abruptly due to viscoleastic effects of the polyurethane at that temperature.

At short beam configuration where the shear effects are more significant, at -10ºC the error of the beam and SSBE elements relative to the experimental values is 26% and 28%, respectively. While the error of the beam element relative to the 3-D and plate elements is 11% and 12%, respectively. At 50ºC the error of the beam element relative to experimentation is 16%, while relative to the 3-D and plate elements is 19% and 20%, respectively. The SSBT element has a 15% error relative to experimental results. Once again at 50ºC the results vary a lot when compared to experimentation because of the viscoelatic effects and in this case are more severe due to the increase in the shear stresses magnitude as a consequence of the short configuration.

The longitudinal strains distribution of specimens S12305 and S12155 along the thickness of the sandwich at the mid-span section are shown in figures 6 and 7.

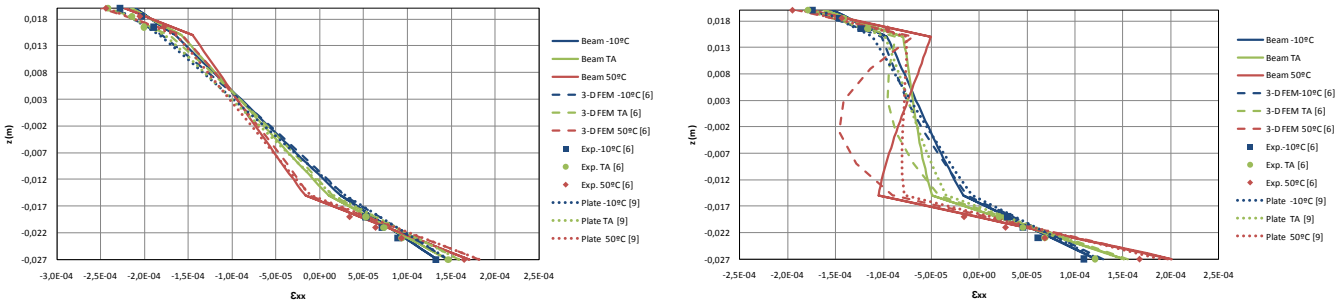

a) b)

Figure 6: Longitudinal strain, ε_{xx}, for S12305 specimen in mid-span section at configuration of a) Long beam; b) Short beam.

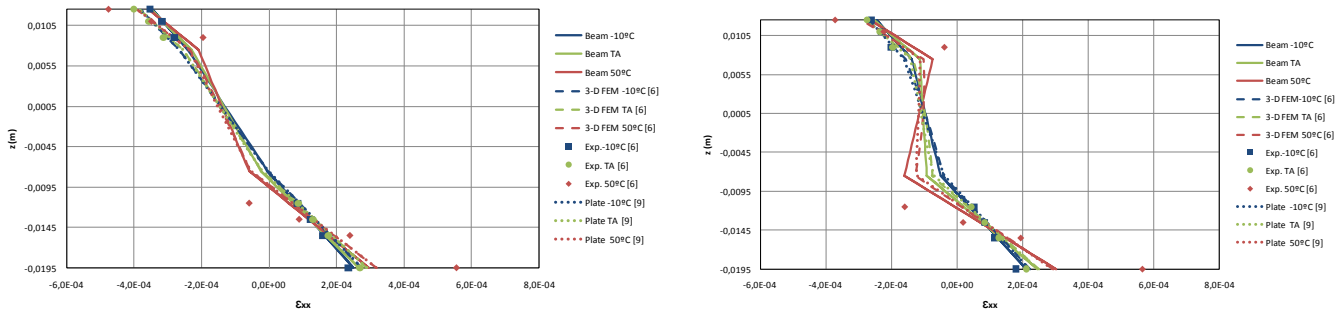

a) b)

Figure 7: Longitudinal strain, ε_{xx}, for S12155 specimen in mid-span section at configuration of a) Long beam; b) Short beam.

From the analysis of the previous figures it can be concluded that for long beam configuration all the models are in accordance. For the short beam configuration the beam and plate elements results are very similar, but when compared to the 3-D element it can be seen that the shear effects are more significant in the specimen S12305, since its core is twice as thick as the S12155 specimen. Despite this there is another effect that is not accounted in the plate and beam elements which is the compressibility. The big warping effect in the 3-D FEM in figure 6.b) is caused by the compression as a consequence of the loading configuration.

4. Conclusions

For short beam configuration the beam element presented here is quite accurate and in accordance with the results obtained by 3-D and plate elements. It also produces better understanding of the strain distributions than the simplified first order element SSBT. Since both the beam and plate models do not take into account in their formulation the compression of the core, the results of the strains in that area produce bigger errors in beams that are thicker when compared to their length. The viscolelastic effects of the polyurethane core, especially at 50ºC, also leads to great discrepancies between the experimental and the models results. It is then desirable not only to include the compressibility effects in the core and beam elements as well as the viscoelastic effects, in order to better simulate the real behavior of sandwich structures with different core rigidities.

References

[1] Allen, H. G., *Analysis and Design of Structural Sandwich Panels*, Pergamon Press, 1969.

[2] Davies, J. M., *Lightweight Sandwich Construction*, Blackwell Publishing, 2001.

[3] Reliability study on the application of Sandwich in the HS 900 Catamaran, http://www.lass.nu/Reports/Sandwich%20Construction%20-%20Application%20on%20a%20Superstructure.pdf, (May 2010).

[4] Boeing 787 Dreamliner – Program Fact Sheet, http://www.boeing.com/commercial/787family/programfacts.html, (May 2010).

[5] Airbus A350XWB, http://www.airbus.com/store/mm_repository/flash/a350xwb/airbus/, (May 2010).

[6] Teixeira de Freitas, S., H. Kolstein, F. Bijlaard, *Sandwich System for Renovation of Orthotropic Steel Bridge Decks*, 9th International Conference on Sandwich Structures, 2010, Pasadena, California, USA.

[7] Vincent, R., A. Ferro, *A New Orthotropic Bridge Deck: Design, Fabrication and Construction of the Shenley Bridge Incorporating an SPS Orthotropic Bridge Deck*, In 2004 Orthotropic Bridge Conference, Sacramento, California, USA, 2004.

[8] Feldmann, M., G. Sedlacek, A. Geler, *A System of Steel-Elastomer Sandwich Plates for Strengthening Orthotropic Bridges Decks*, Mechanics of Composite Materials, 2007; 43 (2): 183–190.

[9] Araújo, A. L., C. M. Mota Soares, C. A. Mota Soares, *Finite Element Model for Hybrid Active-Passive Damping Analysis of Anisotropic Laminated Sandwich Structures*, Journal of Sandwich Structures and Materials, 2010; 12:397-419.

[10] Araújo, A.L., C.M. Mota Soares, J. Herskovits, P. Pedersen, *Development of a Finite Element Model for the Identification of Mechanical and Piezoelectric Properties Through Gradient Optimization and Experimental Vibration Data*, Composite Structures, 2002; 58: 307-318.

[11] Reddy, J. N., *Mechanics of Laminated Composite Plates and Shells: Theory and Analysis*, 2nd Edition, CRC Press, 2004, Boca Raton, USA.

[12] Reddy, J. N., *An Introduction to the Finite Element Method*, 3rd Edition, McGraw-Hill, 2005.

[13] ASTM-C393, *C393-06: Standard Test Method for Core Shear Properties of Sandwich Constructions by Beam Flexure*, 2006.

[14] Mead, D.S., S. Markus, *The Forced Vibration of a Three-Layer Damped Sandwich Beam With Arbitrary Boundary Conditions*, Journal of Sound and Vibration, 1969; 10(2): 163-175.

[15] Sainsbury, M.G., Q.J. Zhang, *The Galerkin Element Method Applied to the Vibration of Damped Sandwich Beams*, Composite and Structures, 1999; 71:239-256.

[16] ISO-527, *EN ISO 527:1996 Plastics – Determination of Tensile Properties*, 1996.